fluids

MDPI

Article

A Comparative Study between Sand- and Gravel-Bed Open Channel Flows in the Wake Region of a Bed-Mounted Horizontal Cylinder

Kalpana Devi [1], Prashanth Reddy Hanmaiahgari [1,*], Ram Balachandar [2] and Jaan H. Pu [3,*]

[1] Department of Civil Engineering, IIT Kharagpur, Kharagpur 721302, India; kalpanarajpoot@iitkgp.ac.in
[2] Department of Civil and Environmental Engineering, University of Windsor, Windsor, ON N9B 3P4, Canada; rambala@uwindsor.ca
[3] School of Engineering, Faculty of Engineering and Informatics, University of Bradford, Bradford BD71DP, UK
* Correspondence: hpr@civil.iitkgp.ac.in (P.R.H.); j.h.pu1@bradford.ac.uk (J.H.P.)

Abstract: In nature, environmental and geophysical flows frequently encounter submerged cylindrical bodies on a rough bed. The flows around the cylindrical bodies on the rough bed are very complicated as the flow field in these cases will be a function of bed roughness apart from the diameter of the cylinder and the flow velocity. In addition, the sand-bed roughness has different effects on the flow compared to the gravel-bed roughness due to differences in the roughness heights. Therefore, the main objective of this article is to compare the mean velocities and turbulent flow properties in the wake region of a horizontal bed-mounted cylinder over the sand-bed with that over the gravel-bed. Three experimental runs, two for the sand-bed and one for the gravel-bed with similar physical and hydraulic conditions, were recorded to fulfil this purpose. The Acoustic Doppler Velocimetry (ADV) probe was used for measuring the three-dimensional (3D) instantaneous velocity data. This comparative study shows that the magnitude of mean streamwise flow velocity, streamwise Reynolds normal stress, and Reynolds shear stress are reduced on the gravel-bed compared to the sand-bed. Conversely, the vertical velocities and vertical Reynolds normal stress are higher on the gravel-bed than the sand-bed.

Keywords: ADV; bed-mounted horizontal cylinder; gravel-bed; sand-bed; turbulence; wake region

Citation: Devi, K.; Hanmaiahgari, P.R.; Balachandar, R.; Pu, J.H. A Comparative Study between Sand- and Gravel-Bed Open Channel Flows in the Wake Region of a Bed-Mounted Horizontal Cylinder. *Fluids* **2021**, *6*, 239. https://doi.org/10.3390/fluids6070239

Academic Editor: Mehrdad Massoudi

Received: 14 May 2021
Accepted: 26 June 2021
Published: 1 July 2021

1. Introduction

Turbulent flows over rough surfaces occur in engineering applications and natural sciences. Determining the roughness effects on the turbulent flows in engineering applications is very important since the mechanisms of production, diffusion, and energy transfer between the mean and the turbulent fields, especially in the near-wall region, are influenced by surface roughness.

There has been considerable work carried out to understand the dynamics of turbulent flows over rough surfaces. The numerous studies in the past, before 1990, are related to the universal aspects of rough-walled flows. Most of them have highlighted the effects of uniformly distributed roughness elements of standard shapes, such as spheres, bars, racks, cylinders, ribs, dunes, and vegetation [1–6]. Though, very recently, a few researchers have focused on illustrating the realistic roughness effects on various features of turbulent flows [7,8]. The realistic roughness is quite different from the regular (or 'modelled') roughness. It is described by a wider spectrum of wavelengths and random distribution of structures of each scale.

Robert et al. [8] and Bigillon et al. [9] analyzed the turbulence statistics on the transitionally rough bed, while Bergstrom et al. [10] investigated the effects of surface roughness on the mean velocity distribution in a turbulent boundary layer. Bergstrom et al. [10] found that the outer flow was significantly affected by the roughness properties. Volino et al. [11]

used two-dimensional roughness fabricated by laying the transverse bars on the channel bed to determine the turbulence structure in a boundary layer. Bomminayuni and Stoesser [12] used a channel bed artificially roughened by hemispheres to analyze the turbulent statistics in the flow. The roughness effects on the near-wall turbulence in terms of Reynolds stress budget were determined numerically by Yuan and Piomelli [13]. Essel and Tachie [14] examined the wall roughness effects on the turbulent flow field downstream of the backward-facing step. They observed a significant reduction in the longitudinal and vertical spatial coherence of the turbulence structures due to the surface roughness. Wu and Piomelli [15] investigated the effects of surface roughness on the separating boundary layer over a flat plate by using large-eddy simulations.

Flow around submerged cylindrical bodies occurs in many environmental and geophysical systems—for example, water, oil, and gas pipelines, a communication cable laid on a river or sea bed, fish habitats, submerged horizontal or vertical pipes, sewer pipelines, hydraulic structures, etc. The flow field around a cylindrical object on a surface has been experimentally and numerically studied extensively in the past for many years. Though, most of the studies determined the wall-proximity effects on the flow characteristics such as the point of separation of wall-boundary layer [16], the drag and lift coefficients [17], the location of front stagnation point [18], distribution of the pressure on the cylinder surface [19], vortical flow structures [20], Strouhal number and vortex shedding phenomenon and flow [21], and turbulence properties of the wake region of the cylinder [22]. A few investigations have analyzed the turbulent flow field of a bed-mounted horizontal cylinder [23–25].

When the cylinder is laid on the rough bed like the sand-bed and gravel-bed, the complexities of the flow may enhance many folds since the flow, in this case, will be a function of bed roughness apart from the diameter of the cylinder and the flow velocity. In addition to that, the flow field on the sand-bed might be quite different from the gravel-bed due to differences in properties of bed roughness.

Due to their practical importance and complexity, several experimental investigations have been carried out to enhance our knowledge of the rough wall turbulent flows. However, there are very few studies that show the effects of gravel-bed roughness on the flow field of a circular cylinder. As per the author's knowledge, there is no comparative investigation between sand and gravel-bed to date to show the effects of bed roughness heterogeneity on the wake flow of the bed-mounted horizontal cylinder. From the literature survey, it is clear that no experimental data are available to understand the bed roughness heterogeneity effects on the mean velocities and turbulent quantities of flow over the cylinder. In addition to that, experimental data are needed to validate the numerical models. Therefore, the present research aims to analyze the roughness heterogeneity effects on the wake region of a bed-mounted circular cylinder in terms of the mean velocities and turbulence quantities.

2. Experimental Details

2.1. Experimental Instrumentations

Experiments were performed in a recirculating rectangular flume (narrow open channel having an aspect ratio less than 5) with dimensions of $L \times B \times H = 12 \times 0.91 \times 0.70$; $12 \times 0.91 \times 0.70$ [25] and $10 \times 0.60 \times 0.65$ for the sand-bed (Run 1 and Run 2) and gravel-bed (GB 1), respectively. The channel bed was provided with a constant longitudinal slope (S_0) of 0.23%, 0.23%, and 0.22% throughout the flume length for Run 1, Run 2, and GB 1, respectively. The experimental set up for Run 1 and Run 2 is the same as used by Devi and Hanmaiahgari [25]. The schematic diagram of the experimental setup with a coordinate system for GB 1 is shown in Figure 1. Photographs of flumes for sand-bed and gravel-bed experiments are shown in Figures 2 and 3. The flume has transparent glass sidewalls to facilitate the visual observation of the flow. The inflow discharge was controlled by a valve and metered by a calibrated V-notch weir located at the inlet tank, upstream of the stilling basin through which the flow enters the flume. The flow depth in the flume was adjusted by controlling tailgate water depth using a tailgate located at the downstream end of the

flume. The cylinder was laid on the flume, covering the entire width of the flume at a distance of 6.5, 6.5, and 5.82 m from the flume inlet for Run 1, Run 2, and GB 1, respectively. The test section was chosen at a distance of 6.3, 6.3, and 5.5 m downstream of the inlet for Run 1, Run 2, and GB 1, respectively. It was ensured that the flow was fully developed in the test section.

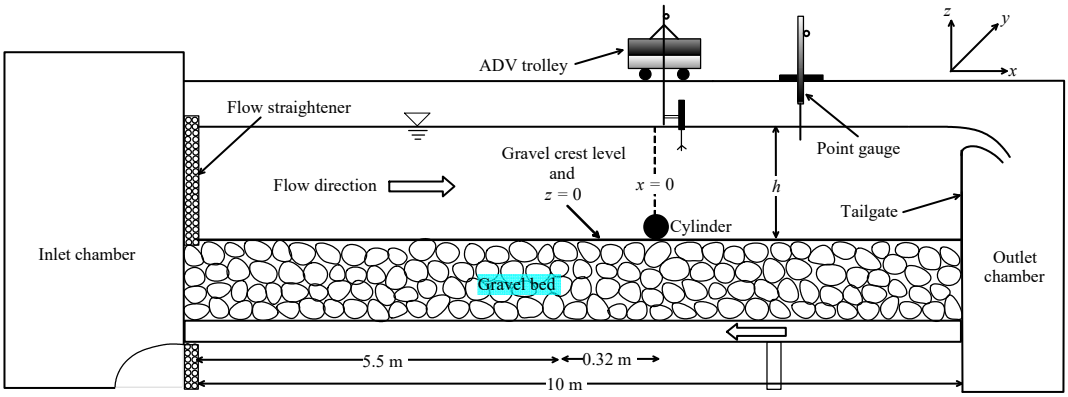

Figure 1. Schematic diagram of the experimental setup for the gravel-bed (GB 1).

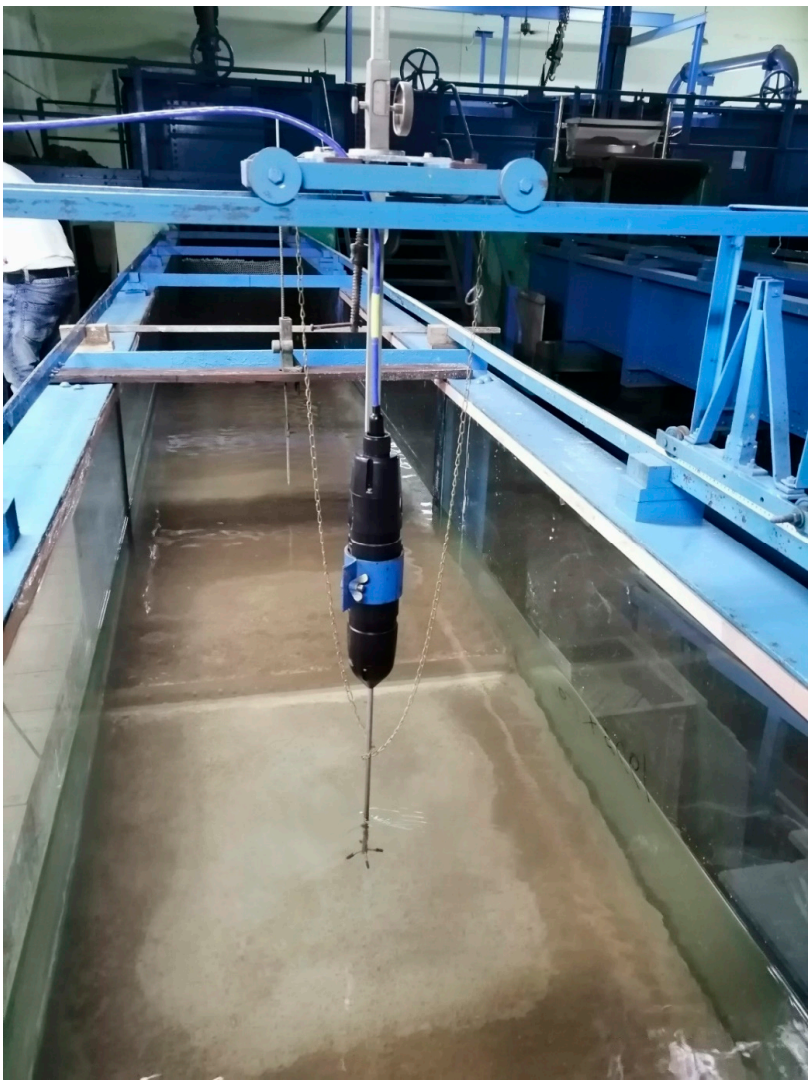

Figure 2. The flume setup for the sand-bed (Run 1 and Run 2).

Figure 3. The flume setup for the gravel-bed (GB 1).

In this study, the x, y, and z axes were oriented in the longitudinal, spanwise, and vertical directions, respectively. The origin of the coordinate system was located at the bottommost point of the cylinder at the central vertical plane in the case of the sand-bed. The origin for the z-axis is the crest level of the top layer of the gravel particles. The nadir of the cylinder is in contact with the crest level. The z is taken positive vertically upwards and negative in the vertically downward direction from the crest level. The bed elevation was measured along the centerline of the flume. The coordinate system for GB 1 along with the schematic diagram of the experimental set up is shown in Figure 1. The time-averaged components of velocity are denoted by $\overline{u}$, $\overline{v}$, and $\overline{w}$ while u, v, and w represent the instantaneous velocity components in the x, y, and z directions, respectively. Here, u', v', and w' symbolize the fluctuating velocity components in the respective directions.

2.2. Bed Settings

The sand-bed (Run 1 and Run 2) was prepared by coating the uniform sand ($d_{50} = 2.54$ mm) over the flume bed. The gravel-bed (GB 1) was fabricated by arbitrarily spreading the well-sorted gravel of median size, $d_{50} = 42.00$ mm in four layers over the flume bed. The gravel particles were spread over the flume bed layer by layer in a compact and packed form. All the gravel particles crests over the gravel-bed were not at the same level as can be seen from the flume set up depicted in Figure 3. The geometric mean size, d_g $(= (d_{84.1}d_{15.9})^{0.5})$ for the sand and gravel are 2.5 and 42.7 mm, respectively. The geometric standard deviation σ_g $(= \sqrt{d_{84.1}/d_{15.9}})$ for both the sand and gravel material was calculated as 1.1. The gradation coefficient G $(= \frac{1}{2}(d_{84.1}/d_{50} + d_{50}/d_{15.9}))$ for the sand sample was 1.10 (< 1.4), which implies that it is uniform sand. Here, $d_{84.1}$ and $d_{15.9}$ represent the size of sediment for which 84.1% and 15.9%, respectively, of the mixture are finer. The particle size distribution curves for the sand-bed (Run 1 and Run 2) and gravel-bed are shown in Figure 4a,b, respectively. A closer look at Figure 4 shows that the sediment size in the case

of the gravel varies over a wider range as compared to the sand. The median size (d_{50}) for the sand and gravel samples are demarcated in Figure 4.

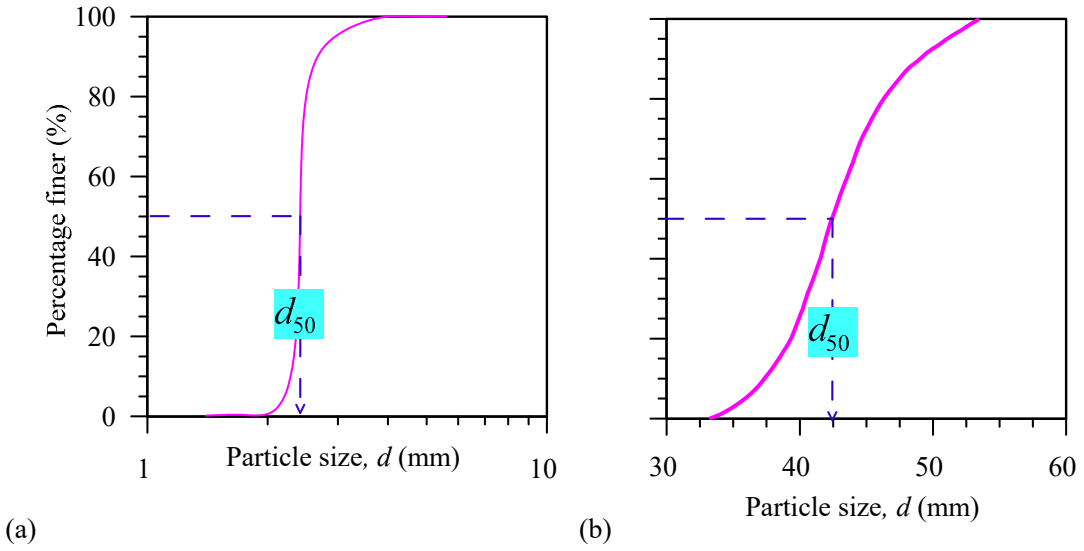

Figure 4. Particle size distribution curve for (**a**) the sand-bed (Run 1 and Run 2) and (**b**) the gravel-bed material (GB 1).

2.3. Experimental Conditions and Measuring Stations

The experiments were conducted under a uniform steady flow condition in a narrow open channel (aspect ratio $Ar < 5$). The experiments were conducted for flow depths (h) of 0.30, 0.30, and 0.25 m for Run 1, Run 2, and GB 1, respectively (Table 1). The flow depth was measured with the help of a point gauge with an accuracy of $\pm$ 0.1 mm by a Vernier scale attachment. The approach flow shear velocity (u_*), which estimates the bed resistance to the flow, was obtained by extrapolating the RSS profile to the flume bed [26]. The values of approach flow shear velocity (u_*) at upstream location ($x = -4D$) for Run 1, Run 2, and GB 1 are 7.1, 9.2, and 27 mm/s, respectively. The hydraulic and physical parameters of all experimental runs (Run 1, Run 2, and GB 1) are given in Table 1. Here, the aspect ratio (Ar) is defined as the ratio of channel width (B) to flow depth (h). For GB 1, the flow depth h was measured with respect to the crest level of the gravel particles, z = 0. Fr is the Froude number ($= \frac{U}{\sqrt{gh}}$) and Re is the flow Reynolds number ($Re = Uh/v$). The shear Reynolds number (R_*) is calculated using Equation (1):

$$R_* = k_s u_* / v \quad (1)$$

where k_s is the equivalent roughness height, and v is the kinematics viscosity of water. Here the median particle size, d_{50} was considered equivalent to the equivalent roughness height, k_s.

Table 1. Hydraulic and physical parameters of all experimental runs (Run 1, Run 2, and GB 1).

Exp. Run	D (m)	S_0(%)	h (m)	U (m/s)	Ar	d_{50}(m)	Re	Re_*	Fr
Run 1	0.05	0.023	0.30	0.15	3.1	0.00254	45,000	18.03	0.09
Run 2	0.05	0.023	0.30	0.19	3.1	0.00254	57,000	23.37	0.11
GB 1	0.06	0.022	0.25	0.25	2.4	0.04200	62,500	1050	0.16

Velocity profiles were measured in the central vertical plane (xz-plane) of the channel at nine ($x = -4D$, 0, $2D$, $3D$, $4D$, $6D$, $8D$, $10D$, and $12D$) different measuring stations in

the longitudinal direction of the flow for all runs. At $x = -4D$, the flow is undisturbed, and it is located upstream of the cylinder. The cylinder is fixed at streamwise location $x = 0$.

2.4. ADV System and Data Collection Procedure

The instantaneous flow velocities were measured by a Three-Dimensional Acoustic Doppler Velocimetry (3D ADV) instrument. A four-receiver down-looking ADV probe, named Vectrino plus (manufactured by Nortek), was used, which significantly reduces the noise signal of the measurements compared to a three-receivers probe [27]. It was functioning with an acoustic frequency of 10 MHz to capture the instantaneous 3D flow velocities, and the sampling rate was 100 Hz as used by Maji et al. [28]. Since the measuring location was 5 cm below the probe, the data acquisition was not possible near the free water surface.

It was ensured that the sampling volume did not touch the flume bed during data collection. The sampling duration was taken as 300 s to ensure that the time-averaged velocities are statistically time-independent. During the experiments, the least value of the signal-to-noise (SNR) ratio and the correlation coefficient were retained as 17 and 70, respectively. The signal captured by the Vectrino in the near-bed flow zone contained spikes due to the interaction between the incident and reflected pulses. Therefore, the raw data were filtered by a spike removal algorithm, known as the phase-space threshold method developed by Goring and Nikora [29].

3. Results and Discussion

The time-averaged longitudinal ($\overline{u}$) and vertical flow velocities ($\overline{w}$) were estimated as an ensemble average of the instantaneous velocities of the respective directions and mathematically expressed by Equations (2) and (3) as used by Devi and Hanmaiahgari [25]:

$$\overline{u} = \frac{1}{N}\sum_{i=1}^{N} u_i \tag{2}$$

$$\overline{w} = \frac{1}{N}\sum_{i=1}^{N} w_i \tag{3}$$

where u_i and w_i indicate the longitudinal and vertical components of instantaneous velocity, respectively, and N is the total number of data samples collected. The method of Reynolds decomposition gives the components of fluctuating velocity in the longitudinal (u') and vertical directions (w') by Equation (4) and (5), respectively as:

$$u' = u_i - \overline{u} \tag{4}$$

$$w' = w_i - \overline{w} \tag{5}$$

Reynolds normal stresses in the longitudinal (σ_{uu}) and vertical (σ_{ww}) directions are expressed as the mean of quadratic product of the fluctuating components of the velocities in the corresponding directions and are evaluated by Equations (6) and (7):

$$\sigma_{uu} = \overline{u'u'} = \frac{1}{N}\sum_{i=1}^{N}(u_i - \overline{u})^2 \tag{6}$$

$$\sigma_{ww} = \overline{w'w'} = \frac{1}{N}\sum_{i=1}^{N}(w_i - \overline{w})^2 \tag{7}$$

Reynolds shear stress per unit mass (τ_{uw}) was estimated by using Equation (8).

$$\tau_{uw} = -\overline{u'w'} = -\frac{1}{N}\sum_{i=1}^{N}(u_i - \overline{u})(w_i - \overline{w}) \tag{8}$$

The maximum longitudinal time-averaged velocity occurs within a 5 cm depth from the water surface. Due to the limitations of the ADV probe, it was not possible to collect data within a 5 cm depth from the water surface. It is assumed that the free surface effect

in the subcritical flows is limited to a very shallow region near the free surface and it will not change underlying hydrodynamics. Therefore, the approach flow maximum velocity (U_{max}) is taken as the maximum velocity of each run at $x = -4D$ from the available data measuring points. The mean and turbulent flow characteristics for all three runs were normalized by the approach flow maximum velocity (U_{max}) and the vertical distances (z) were normalized by the flow depth (h). The normalized vertical distance is denoted by $\bar{z}$ ($= z/h$). The normalized mean velocities, normalized RNS, and normalized RSS were plotted against normalized vertical distance ($\bar{z}$) for Run 1 and Run 2 together, and GB 1 separately at all nine measuring stations. The plots are analyzed and compared to examine the surface roughness effects on the wake region of the cylinder.

The entire flow field of the cylinder is divided into three flow zones, namely undisturbed upstream, recirculation region, and redevelopment region, as used by Essel and Tachie [30] in the case of forward-facing step. The recirculation and redevelopment regions are in the wake region of the cylinder. The measuring station $x = -4D$ is located upstream of the cylinder; $x = 2D$, $3D$, $4D$, and $6D$ are in the recirculation region; and $x = 8D$, $10D$, and $12D$ fall in the redevelopment region. It is noteworthy to mention that the flow is still under the recovery process at $x = 12D$, and it is not yet fully recovered. A schematic of the upstream, recirculation, and redevelopment regions of a circular cylinder is shown in Figure 5.

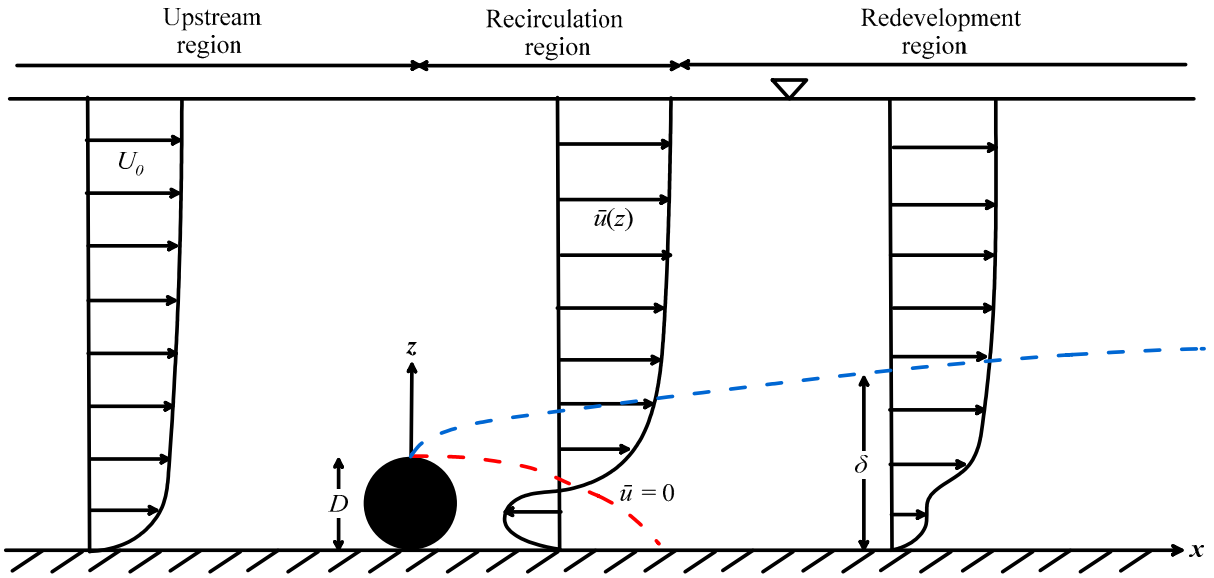

Figure 5. Schematic of different regions of flow field upstream and downstream of a circular cylinder.

The main findings of the proposed experimental research are discussed below.

3.1. Mean Velocities

The time-averaged velocities in the longitudinal ($\overline{u}$) and vertical directions ($\overline{w}$) are normalized by the approach flow maximum velocity (U_{max}) and are written as $\overline{u}/U_{max}$ and $\overline{w}/U_{max}$, respectively. Figure 6 examines the vertical profiles of normalized time-averaged longitudinal velocity ($\overline{u}/U_{max}$) for Run 1, Run 2, and GB 1.

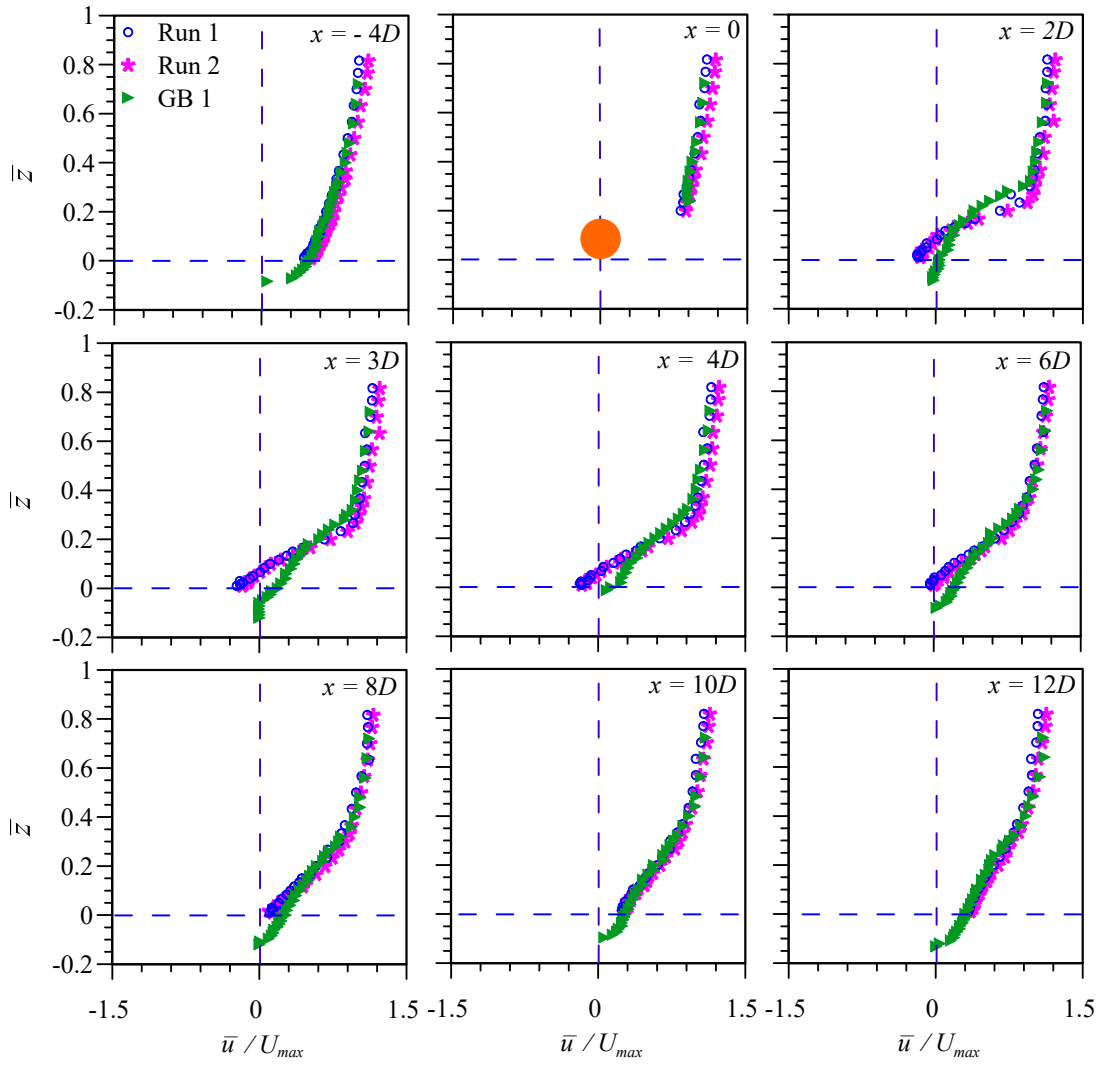

Figure 6. The vertical profiles of normalized time-averaged longitudinal velocity ($\overline{u}/U_{max}$) at different measuring stations (x) for Run 1, Run 2, and GB 1.

From Figure 6, it is clearly visible that the streamwise velocity is higher for Run 2 compared to Run 1. The former case has a higher Reynolds number (Re) compared to the latter, resulting in higher streamwise velocity. It is also observed that at upstream undisturbed location ($x = -4D$), the vertical profile of $\overline{u}/U_{max}$ for both types of beds follows logarithmic law. All the velocity profiles in the wake region preserve no-slip conditions. No negative longitudinal velocity is observed in the near-bed flow of the recirculation region over the gravel-bed, which shows a diminished separation zone on the gravel-bed. This observation is contrary to the observation made in the case of the sand-bed, where the longitudinal velocity in the near-bed flow of the recirculation region is negative in magnitude. This comparative study shows that the magnitude of mean streamwise flow velocity is smaller on the gravel-bed than the sand-bed, although the Reynolds number is higher for the flow on the gravel-bed (Figure 6). Figure 6 infers that the gravel-bed profiles are 'less full' than the sand-bed profiles. This phenomenon is similar to a reduction in longitudinal velocity due to roughness upstream and downstream of the rough backward-facing step (Wu et al. [31]). A closer look at Figure 6 shows that the vertical location of a point of inflection ($d^2u/dz^2 = 0$) in the $\overline{u}/U_{max}$ distribution is higher in the case of the gravel-bed ($\overline{z} \approx 0.30$) as compared to the sand-bed ($\overline{z} \approx 0.25$). Hence, it is concluded that the vertical location of the point of inflection ($d^2u/dz^2 = 0$) for the gravel-bed shifted away from the bed, implying a decrease in the longitudinal near-bed

velocity caused by the gravel-bed roughness and increase in the thickness of roughness sublayer on the gravel-bed.

Figure 7 depicts the variation of normalized time-averaged vertical velocity ($\overline{w}/U_{max}$) against normalized vertical distance ($\overline{z}$) at different measuring stations (x) for Run 1, Run 2, and GB 1. It is very clear from Figure 7 that the vertical velocity is higher for Run 2 compared to Run 1 throughout the vertical domain. In the upstream of the cylinder ($x = -4D$), on the sand-bed, $\overline{w}/U_{max}$ starts with a small positive value and increases very slowly with $\overline{z}$ and becomes almost constant with $\overline{z}$ above $\overline{z} \approx 0.2$. Unlike the sand-bed, in the case of gravel, the $\overline{w}/U_{max}$ starts below the gravel-bed with a small positive value, then suddenly changes to a negative value and then with a further rise in $\overline{z}$, its negative value declines, and it becomes positive for $\overline{z} \geq 0.06$. Thereafter, the vertical velocity increases slowly with vertical distance and become almost invariant of $\overline{z}$ like over the sand-bed. It is also observed that for $x = -4D$, 0, and $2D$, the profiles are positive on both the sand and gravel-beds with an exception at $x = -4D$ on the gravel-bed. As already mentioned, at $x = -4D$ on the gravel-bed, below the bed level velocity is negative up to $\overline{z} \approx 0.06$. In the wake region, the vertical velocity starts with a small negative value and then increases (negative value) abruptly with a rise in $\overline{z}$ and attains a negative peak. Thereafter, the negative value quickly declines with an increase in vertical distance from the bed and become almost constant with $\overline{z}$ variation above $\overline{z} \approx 0.4$. These patterns in the $\overline{w}/U_{max}$ distribution is similar on the sand and gravel-beds for the wake region with an exception at $x = 2D$. At $x = 2D$, for both beds, the $\overline{w}/U_{max}$ profiles are completely positive, unlike at other locations, where they are negative. The vertical location of the peak at $x = 2D$ on the sand-bed corresponds to the top level of the cylinder ($z \approx 1$), while this is not true over the gravel-bed. The vertical location of the peak of $\overline{w}/U_{max}$ over the gravel-bed has shifted away from the bed due to the damping of the longitudinal velocity resulting from the heterogeneity of the gravel-bed. In the recirculation region, the vertical location of the peak of $\overline{w}/U_{max}$ shifted towards the bed with the increase in x. On the contrary, in the redevelopment region, for both the sand and gravel-beds, the vertical location of the peak moved away from the bed with an increase in x. In the recirculation region, the magnitude of the negative peak of $\overline{w}/U_{max}$ increases in the streamwise direction with x. Conversely, the declining patterns in the magnitude of the negative peak with an increase in x are observed in the redevelopment region for both the sand and gravel-beds. The location of peak ($\overline{z} > 0.4$) on the gravel-bed is higher than the location of the peak ($\overline{z} < 0.4$) on the sand-bed. It is clearly observed from Figure 7 that the maximum negative vertical mean velocity on the sand-bed and gravel-bed is about $0.1U_{max}$ and $0.05U_{max}$, respectively. Hence, an inference is made that gravel-bed roughness has dampened the value of the maximum negative vertical mean velocity.

3.2. Reynolds Normal Stress (RNS) Distribution

The Reynolds normal stresses (RNSs) define the strength of the turbulence and give an idea about the fluctuating velocity components. The RNSs are affected by factors such as velocity, roughness size, roughness orientation, etc. These are denoted as σ_{uu} and σ_{ww} in the longitudinal (x) and vertical (z) directions, respectively. They are normalized by the approach flow maximum velocity ${U_{max}}^2$ and are given as $\sigma_{uu}/{U_{max}}^2$ and $\sigma_{ww}/{U_{max}}^2$, respectively. The normalized streamwise ($\sigma_{uu}/{U_{max}}^2$) and vertical ($\sigma_{ww}/{U_{max}}^2$) RNSs are plotted against the normalized vertical distance ($\overline{z}$) for all the three runs (Run 1, and Run 2, and GB 1) in Figures 8 and 9, respectively, at different measuring stations (x).

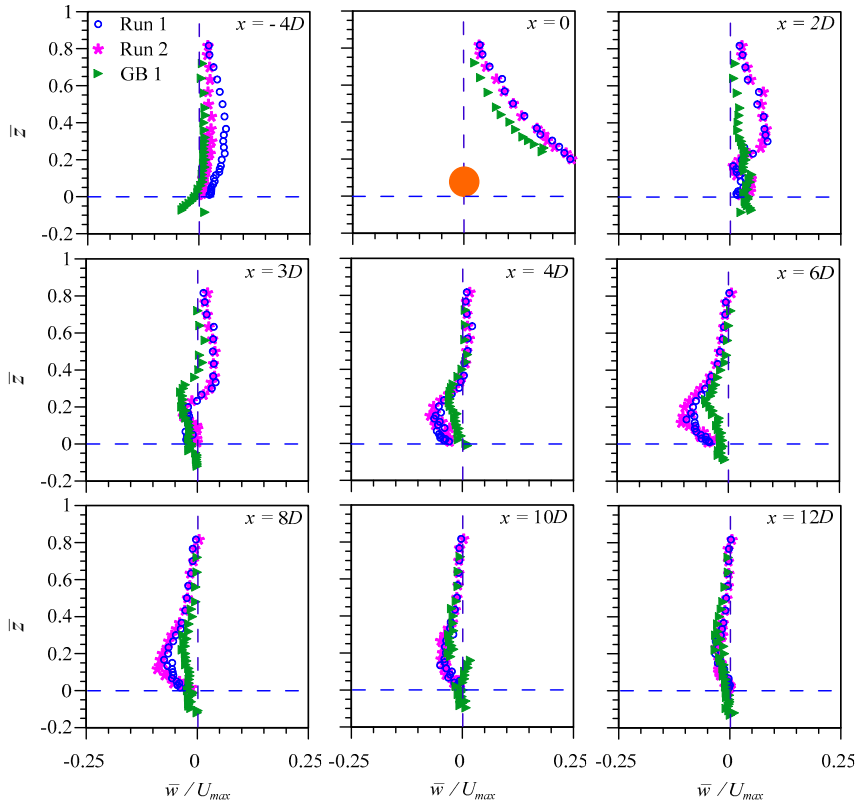

Figure 7. The variation of normalized time-averaged vertical velocity ($\overline{w}/U_{max}$) against normalized vertical distance ($\overline{z}$) at different measuring stations (x) for Run 1, Run 2, and GB 1.

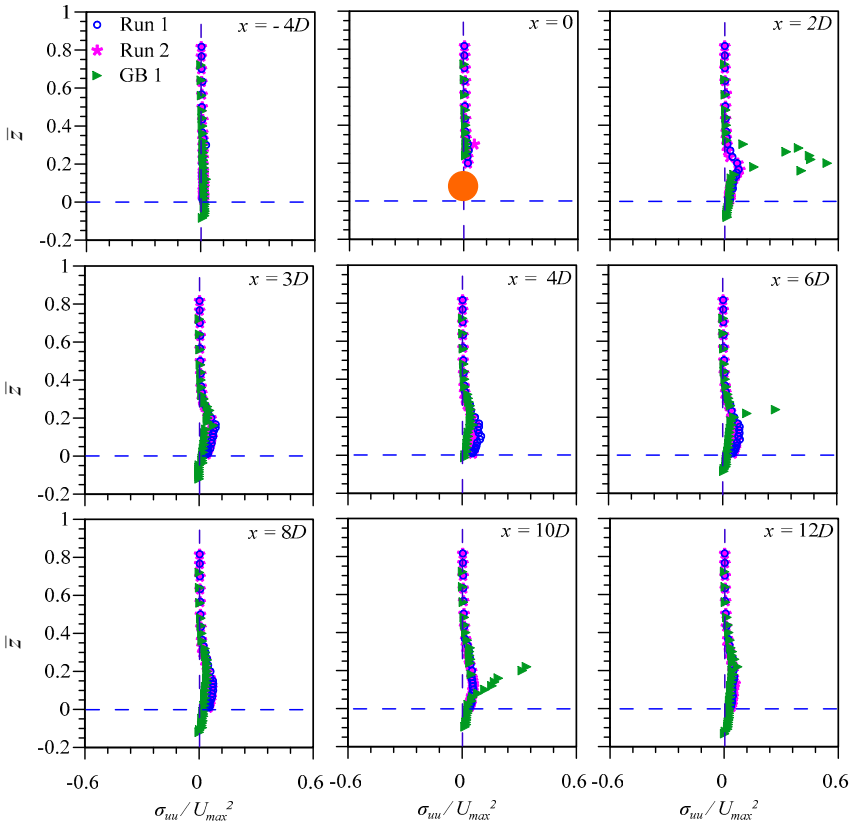

Figure 8. The vertical profiles of normalized longitudinal RNS ($\sigma_{uu}/{U_{max}}^2$) at different measuring stations (x) for Run 1, Run 2, and GB 1.

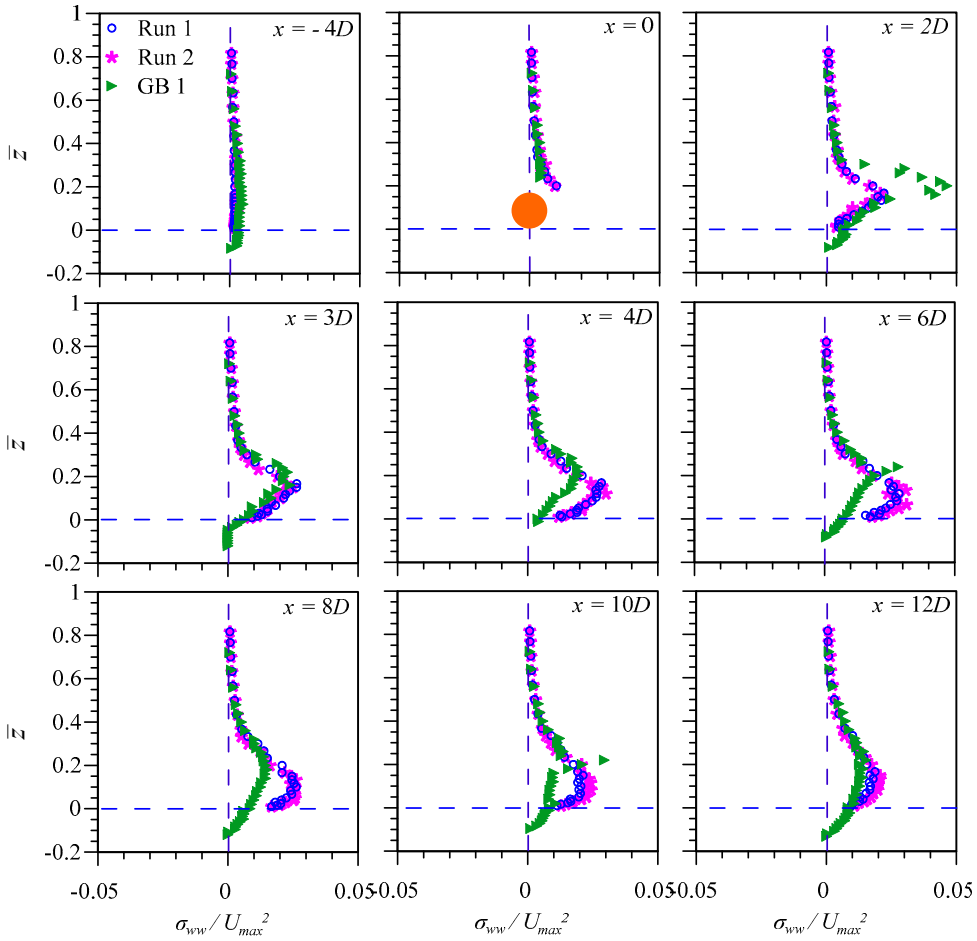

Figure 9. The variation of normalized time-averaged vertical RNS ($\sigma_{ww}/U_{max}{}^2$) against normalized vertical distance ($\bar{z}$) at different measuring stations (x) for Run 1, Run 2, and GB 1.

From Figures 8 and 9, it is noticed that the value of both σ_{uu} and σ_{ww} are higher in the case of Run 2 compared to Run 1. It is observed that in the uninterrupted upstream flow ($x = -4D$), the $\sigma_{uu}/U_{max}{}^2$ and $\sigma_{ww}/U_{max}{}^2$ profiles demonstrate diminishing trends against a rise in the $\bar{z}$ over the sand and gravel-beds. In the recirculation region, $\sigma_{uu}/U_{max}{}^2$ and $\sigma_{ww}/U_{max}{}^2$ start with a small positive value and increase sharply with the rise in $\bar{z}$ and attain a peak. Thereafter, it declines abruptly with further increase in $\bar{z}$ and then attains a small positive value and becomes almost invariant with $\bar{z}$. In the recirculation region ($x = 2D$, $3D$, $4D$, and $6D$), the vertical locations of the peaks of normal stresses are occurring near the bed. In contrast, they shifted away from the bed in the redevelopment region for both the sand- and gravel-bed flows. Their peaks were increasing in the recirculation region, but they decrease in the redevelopment region for both the sand- and gravel-bed flows. However, it is observed that the magnitudes of $\sigma_{uu}/U_{max}{}^2$ peaks on the gravel-bed are smaller than the sand-bed. Contrary to this, the peaks of $\sigma_{ww}/U_{max}{}^2$ on the gravel-bed are larger than the sand-bed. The gravel-bed roughness considerably diminished $\sigma_{uu}/U_{max}{}^2$ in both the recirculation and redevelopment regions compared to the sand-bed, which is similar to the observation of Wu et al. [31]. Although, $\sigma_{ww}/U_{max}{}^2$ are enhanced significantly on the gravel-bed as compared to the sand-bed in both the regions, which is contrary to the observation of Wu et al. [31]. In fact, Wu et al. [31] have observed that due to forward-facing step roughness, the RNS decreased downstream of the step. Furthermore, $\sigma_{uu}/U_{max}{}^2$ on the gravel-bed is more significantly diminished as compared to the increase in $\sigma_{ww}/U_{max}{}^2$ on the gravel-bed. In Figure 8, $\sigma_{uu}/U_{max}{}^2$ profiles over GB 1 show kinks at X/D = 2, 6, and 10 at z/h = 0.2, which is attributed to measurement error at that location. Finally, it is concluded that the peak normal stresses (turbulence

intensities) show increasing trends in the recirculation region and decreasing patterns in the reattached region due to the enhanced turbulence in the former region and the attenuation of turbulence in the latter region.

3.3. Reynolds Shear Stress (RSS)

The Reynolds shear stress (RSS) is the time-averaged value of the quadratic terms of the fluctuating velocities components. The Reynolds shear stress has a similar influence on the flow as viscosity. The RSS offers resistance to the flow in the corresponding plane and governs secondary flows. The RSS in the xz plane per unit weight is denoted as τ_{uw} and the RSS normalized by the approach flow maximum velocity ($U_{max}{}^2$) is written as $\tau_{uw}/U_{max}{}^2$. The vertical profiles of normalized RSS ($\tau_{uw}/U_{max}{}^2$) at different measuring stations (x) for Run 1, Run 2, and GB 1 are shown in Figure 10.

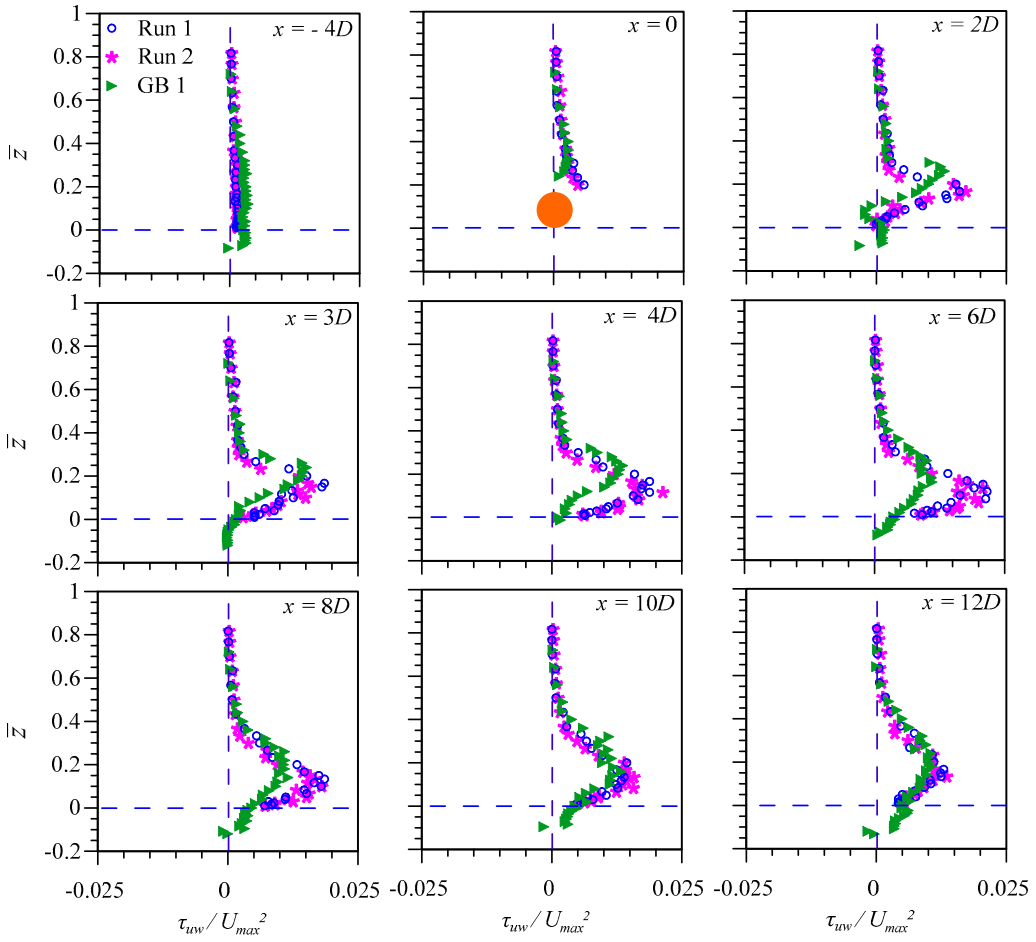

Figure 10. The vertical profiles of normalized RSS ($\tau_{uw}/U_{max}{}^2$) at different measuring stations (x) for Run 1, Run 2, and GB 1.

As evident from Figure 10, RSS is higher for Run 2 compared to Run 1 throughout the study domain. In the upstream of the cylinder, the RSS varies linearly with the vertical distance for both sand-bed and gravel-bed. The RSS magnitude in the wake region is slightly smaller on the gravel-bed than the sand-bed, although the Reynold number (Re) is considerably higher in the former case than the latter. The vertical location of the RSS peak is more elevated on the gravel-bed in the wake flow, which shows that roughness is extended farther in the gravel-bed flows. Interestingly, peaks of RSS are occurring at the top level of the cylinder on the sand-bed. In the recirculation region, $\tau_{uw}/U_{max}{}^2$ starts with a small positive value and increases sharply with a rise in the vertical distance and attains a peak much above the cylinder height. After that, it reduces sharply with a further rise in

$\bar{z}$ from the bed, then attains a minimal positive value and becomes almost invariant with $\bar{z}$. In the recirculation region ($x = 2D$, $3D$, $4D$, and $6D$), the vertical location of the peak of the RSS shifted towards the bed. In contrast, the peak is moved away from the bed for both the beds in the redevelopment region. The magnitude of the $\tau_{uw}/{U_{max}}^2$ peak increases in the recirculation region, but it decreases in the redevelopment region for both the sand- and gravel-bed flows. In the wake flow, the peak of RSS is occurring at $\bar{z} \approx 0.2$ for $x = 2D$ while moving away from the cylinder, and the vertical location of the peak is shifted towards the bed. The RSS peaks values are declining along the streamwise direction downstream of the cylinder over both the sand-bed and gravel-bed. This finding on the gravel-bed is similar to the flow pattern downstream of the rough forward-facing step (Wu et al. [31]).

4. Conclusions

This analysis conveys a clear understanding that gravel-bed roughness in comparison to sand-bed roughness significantly modifies the turbulence levels downstream of a horizontally mounted cylinder. In addition to that, the higher values of streamwise velocity, vertical velocity, RNSs, and RSS were observed in the case of a higher Reynolds number flow over the sand-bed due to a higher level of turbulence. In contrast, for similar Reynolds flow over sand- and gravel-beds, turbulence statistics such as RNSs and RSS are higher on the sand-bed than the gravel-bed. The peak values of streamwise velocity, vertical velocity, RSS, and RNSs have been dampened by the gravel-bed roughness. The enhanced roughness over the gravel-bed shifts the location of the peak of vertical velocity over the gravel-bed away from the flume bed compared to the location of the peak of vertical velocity over the sand-bed. Similarly, the vertical location of the point of inflection in the streamwise velocity profile is higher in the case of the gravel-bed than the sand-bed. The peak RNSs and RSS show increasing trends in the recirculation region and decreasing patterns in the reattached region over and sand- and gravel-beds. Finally, it is observed that the flow is mainly affected in the near-bed region downstream of a cylinder over and sand- and gravel-beds. The proposed research findings are important for the validation of numerical modelling results and improvement of the current numerical models.

Author Contributions: K.D.: writing—original draft preparation, writing—review and editing, and data curation; P.R.H.: writing—original draft preparation, writing—review and editing, funding acquisition, project administration, data curation, and supervision; R.B.: writing—review and editing, data curation, and funding acquisition; J.H.P.: writing—review and editing, funding acquisition and data curation. All authors contributed to the work. All authors have read and agreed to the published version of the manuscript.

Funding: The Author Ram Balachandar acknowledges the grant support from Natural Sciences and Engineering Research Council of Canada the author Jaan H. Pu acknowledges the grant support from the Hidden Histories of Environmental Science Project (at Seedgrant Stage) by the Natural Environment Research Council (NERC) and Arts and Humanities Research Council (AHRC), part of UK Research and Innovation (UKRI).

Institutional Review Board Statement: Not applicable.

Informed Consent Statement: Not applicable.

Data Availability Statement: The data presented in this study are available on reasonable request from the corresponding author.

Conflicts of Interest: The authors declare no conflict of interest.

References

1. Tachie, M.F.; Bergstrom, D.J.; Yang, Z.; Fang, X.; Wang, B.-C. Highly-disturbed turbulent flow in a square channel with V-shaped ribs on one wall. *Int. J. Heat Fluid Flow* **2015**, *56*, 182–197. [CrossRef]
2. Tsikata, J.M.; Tachie, M.F.; Katopodis, C. Open-channel turbulent flow through bar racks. *J. Hydraul. Res.* **2014**, *52*, 630–643. [CrossRef]
3. Balachandar, R.; Bhuiyan, F. Higher-Order Moments of Velocity Fluctuations in an Open-Channel Flow with Large Bottom Roughness. *J. Hydraul. Eng.* **2007**, *133*, 77–87. [CrossRef]

4. Djenidi, L.; Antonia, R.A.; Amielh, M.; Anselmet, F. A turbulent boundary layer over a two-dimensional rough wall. *Exp. Fluids* **2008**, *44*, 37–47. [CrossRef]
5. Krogstad, P.Å.; Andersson, H.I.; Bakken, O.M.; Ashrafian, A. An experimental and numerical study of channel flow with rough walls. *J. Fluid Mech.* **2005**, *530*, 327–352. [CrossRef]
6. Wu, Y.; Ren, H. On the impacts of coarse-scale models of realistic roughness on a forward-facing step turbulent flow. *Int. J. Heat Fluid Flow* **2013**, *40*, 15–31. [CrossRef]
7. Ren, H.; Wu, Y. Turbulent boundary layers over smooth and rough forward-facing steps. *Phys. Fluids* **2011**, *23*, 045102. [CrossRef]
8. Robert, A.; Roy, A.G.; Serres, B. De Turbulence at a roughness transition in a depth limited flow over a gravel bed. *Geomorphology* **1996**, *16*, 175–187. [CrossRef]
9. Bigillon, F.; Nino, Y.; Garcia, M. Measurements of turbulence characteristics in an open-channel flow over a transitionally-rough bed using particle image velocimetry. *Exp. Fluids* **2006**, *41*, 857–867. [CrossRef]
10. Bergstrom, D.J.; Kotey, N.A.; Tachie, M.F. The effects of surface roughness on the mean velocity profile in a turbulent boundary layer. *J. Fluids Eng. Trans. ASME* **2002**, *124*, 664–670. [CrossRef]
11. Volino, R.J.; Schultz, M.P.; Flack, K.A. Turbulence structure in a boundary layer with two-dimensional roughness. *J. Fluid Mech.* **2009**, *635*, 75–101. [CrossRef]
12. Bomminayuni, S.; Stoesser, T. Turbulence Statistics in an Open-Channel Flow over a Rough Bed. *J. Hydraul. Eng.* **2011**, *137*, 1347–1358. [CrossRef]
13. Yuan, J.; Piomelli, U. Roughness effects on the Reynolds stress budgets in near-wall turbulence. *J. Fluid Mech.* **2014**, *760*, 1–12. [CrossRef]
14. Essel, E.E.; Tachie, M.F. Roughness effects on turbulent flow downstream of a backward facing step. *Flow, Turbul. Combust.* **2015**, *94*, 125–153. [CrossRef]
15. Wu, W.; Piomelli, U. Effects of surface roughness on a separating turbulent boundary layer. *J. Fluid Mech.* **2018**, *841*, 552–580. [CrossRef]
16. Agbaglah, G.; Mavriplis, C. Three-dimensional wakes behind cylinders of square and circular cross-section: Early and long-time dynamics. *J. Fluid Mech.* **2019**, *870*, 419–432. [CrossRef]
17. Zhou, B.; Wang, X.; Guo, W.; Gho, W.M.; Tan, S.K. Experimental study on flow past a circular cylinder with rough surface. *Ocean Eng.* **2015**, *109*, 7–13. [CrossRef]
18. Cao, S.; Ozono, S.; Tamura, Y.; Ge, Y.; Kikugawa, H. Numerical simulation of Reynolds number effects on velocity shear flow around a circular cylinder. *J. Fluids Struct.* **2010**, *26*, 685–702. [CrossRef]
19. Cao, S.; Ozono, S.; Hirano, K.; Tamura, Y. Vortex shedding and aerodynamic forces on a circular cylinder in linear shear flow at subcritical Reynolds number. *J. Fluids Struct.* **2007**, *23*, 703–714. [CrossRef]
20. Akoz, M.S. Flow structures downstream of the horizontal cylinder laid on a plane surface. *Proc. Inst. Mech. Eng. Part C J. Mech. Eng. Sci.* **2009**, *223*, 397–413. [CrossRef]
21. Gu, F.; Wang, J.S.; Qiao, X.Q.; Huang, Z. Pressure distribution, fluctuating forces and vortex shedding behavior of circular cylinder with rotatable splitter plates. *J. Fluids Struct.* **2012**, *28*, 263–278. [CrossRef]
22. Ikegaya, N.; Morishige, S.; Matsukura, Y.; Onishi, N.; Hagishima, A. Experimental study on the interaction between turbulent boundary layer and wake behind various types of two-dimensional cylinders. *J. Wind Eng. Ind. Aerodyn.* **2020**, *204*, 104250. [CrossRef]
23. Akoz, M.S.; Sahin, B.; Akilli, H. Flow characteristic of the horizontal cylinder placed on the plane boundary. *Flow Meas. Instrum.* **2010**, *21*, 476–487. [CrossRef]
24. Kirkgoz, M.S.; Oner, A.A.; Akoz, M.S. Numerical modeling of interaction of a current with a circular cylinder near a rigid bed. *Adv. Eng. Softw.* **2009**, *40*, 1191–1199. [CrossRef]
25. Devi, K.; Hanmaiahgari, P.R. Experimental analysis of turbulent open channel flow in the near-wake region of a surface-mounted horizontal circular cylinder. In Proceedings of the River Flow 2020: Proceedings of the 10th Conference on Fluvial Hydraulics, Delft, The Netherlands, 7–10 July 2020; pp. 194–202.
26. Pu, J.H. Velocity Profile and Turbulence Structure Measurement Corrections for Sediment Transport-Induced Water-Worked Bed. *Fluids* **2021**, *6*, 86. [CrossRef]
27. Blanckaert, K.; Lemmin, U. Means of noise reduction in acoustic turbulence measurements. *J. Hydraul. Res.* **2006**, *44*, 3–17. [CrossRef]
28. Maji, S.; Pal, D.; Hanmaiahgari, P.R. Hydrodynamics and turbulence in emergent and sparsely vegetated open channel flow. *Environ. Fluid Mech.* **2017**, *17*, 853–877. [CrossRef]
29. Goring, D.G.; Nikora, V.I. Despiking Acoustic Doppler Velocimeter Data. *J. Hydraul. Eng.* **2002**, *128*, 117–126. [CrossRef]
30. Essel, E.E.; Tachie, M.F. Upstream roughness and Reynolds number effects on turbulent flow structure over forward facing step. *Int. J. Heat Fluid Flow* **2017**, *66*, 226–242. [CrossRef]
31. Wu, Y.; Ren, H.; Tang, H. Turbulent flow over a rough backward-facing step. *Int. J. Heat Fluid Flow* **2013**, *44*, 155–169. [CrossRef]